FUNDAMENTAL STUDIES OF NEURAL STIMULATING ELECTRODES

Ninth Quarterly Report
Covering Period August 29, 1996 to November 28, 1996

CONTRACT NO. N01-NS-4-2310

S. F. Cogan
U. M. Twardoch
G. S. Jones
R. B. Jones
Y. P. Liu

EIC Laboratories, Inc.
111 Downey Street
Norwood, Massachusetts 02062

Prepared for

National Institutes of Health
National Institute of Neurological
Disorders and Stroke
Bethesda, Maryland 20892

February 13, 1997

TABLE OF CONTENTS

LIST OF FIGURES

I. INTRODUCTION AND SUMMARY

This report describes work on NINDS Contract No. N01-NS-4-2310 during the period August 29, 1996 to November 28, 1996. As part of the Neural Prosthesis Program, the broad objectives of the present fundamental studies are: 1) to evaluate the electrochemical processes that occur at the electrode-electrolyte interface during pulsing regiments characteristic of neural prosthetic applications; 2) to establish charge injection limits of stimulation electrode materials which avoid irreversible electrochemical reactions; 3) to develop an *in vitro* method, which can be applied *in vivo*, for determining the electrochemical real area and stability of microelectrodes; 4) to develop new materials which can operate at high stimulation charge densities for microstimulation; and 5) to provide electrochemical and analytical support for other research activities in the Neural Prosthesis Program at NINDS.

During this reporting period, long term stability studies of U. Michigan ribbon-cable probe No. 1, site 1 were continued. The apparent capacitance of the unactivated site, calculated from the current at 0.0 V vs. Ag/AgCl in a 200 V/s potential sweep, has been monitored for over 406 days of soaking in PBS. An abrupt but modest increase in the capacitance from 0.5 nF to ~2.5 nF was observed at day 91 of the soak test. On day 217 of the soak test, the electrode was inadvertently allowed to dry out. After the electrode was rehydrated, the apparent capacitance had decreased to a value closer to that observed before day 91. There has been no increase in C_{app}, similar to that observed at day 91, for the 189 days of soaking since the electrode was rehydrated at day 217. This result suggests that the increase in C_{app} at day 91 is not due to an ongoing degradation process at the electrode. This electrode site has exhibited good stability in PBS for well over one year.

The affect of activation potential limits and pulse duration on the uniformity and growth rate of AIROF has been evaluated. Our studies suggest that uniform activation can be achieved with potential pulse activation provided the dwell time at each potential limit is long enough for the activation current to reach background levels. A dwell time of 10 s, compared with the more typical value of 0.5 s, appears effective in providing uniform activation of large area (~0.1 mm^2)

electrodes. Cathodic and anodic potential limits of -0.7 V and 0.95 V vs. AgIAgCl resulted in the highest AIROF activation rates in PBS.

Studies on graded Ti-Ir interfaces for enhancing adhesion and preventing delamination of thin sputtered Ir films continued this quarter. Electrodes with discrete Ti/Ir interfaces, discrete Ti/TiIr alloy interfaces, and graded interfaces were evaluated by activation in 0.3 M Na_2HPO_4 using a 10 s dwell at potential limits of -0.755 V and 0.795 V vs. AgIAgCl. During the course of the activation, the electrodes were characterized by cyclic voltammetry from which charge storage capacity (CSC) was obtained by integration of 0.05 V/s potential sweeps between the activation limits. Two compositional profiles that produced a marked increase in stability were identified. These compositional profiles allowed the electrodes to be activated for 10,000 pulses to a CSC of 50-80 mC/cm^2 without visible evidence of AIROF delamination. With the same activation protocol, discrete interface electrodes failed by delamination after 1300 pulses.

2. VOLTAMMETRIC STUDIES ON Ir MICROELECTRODES

During this quarter we continued studies of the long term stability of Ir sites on a probe with an integrated ribbon cable received from U. Michigan. Figure 2.1 is a diagrammatic representation of the probe showing the numbering scheme for the electrode sites. The probe has been under soak in phosphate buffered saline (PBS) for 406 days.

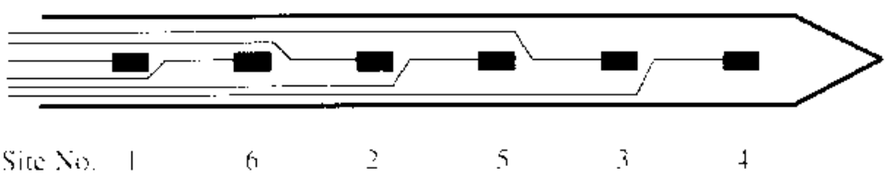

Figure 2.1 Diagrammatic representation of sites and site identification on U. Michigan ribbon-cable probe.

Measurements of the apparent capacitance of site 1 of the ribbon-cable-probe No. 1 were continued. Test procedures and results are detailed in previous Quarterly Progress Reports (Nos. 5-8). Table 2-1 lists the background current obtained from the two studies performed this quarter along with the data from the 23 studies conducted during the previous four quarters. The apparent capacitance, C_{app}, at 200 V/s, is plotted in Fig. 2-2 as a function of time. C_{app} is

calculated by dividing the current at 0.0 V vs. Ag/AgCl by the scan rate, thus $C_{app} = Q/V = i/v$, where v is the scan rate.

Table 2-1 Current measurements for the scan rate studies on site 1 of U. Michigan ribbon-cable probe No. 1, Site 1.

Study No	Days Soaked	Current at 200 V/s (nA)
1	0	79.5
2	8	126
3	35	134
4	52	138
5	59	130
6	70	129
7	76	127
8	91	264
9	100	365
10	108	400
11	135	430
12	143	508
13	150	492
14	160	605
15	164	485
16	164	510
17	171	500
18	203	415
19	220	224
20	227	185
21	233	225
22	246	170
23	272	185
24	354	195
25	406	225

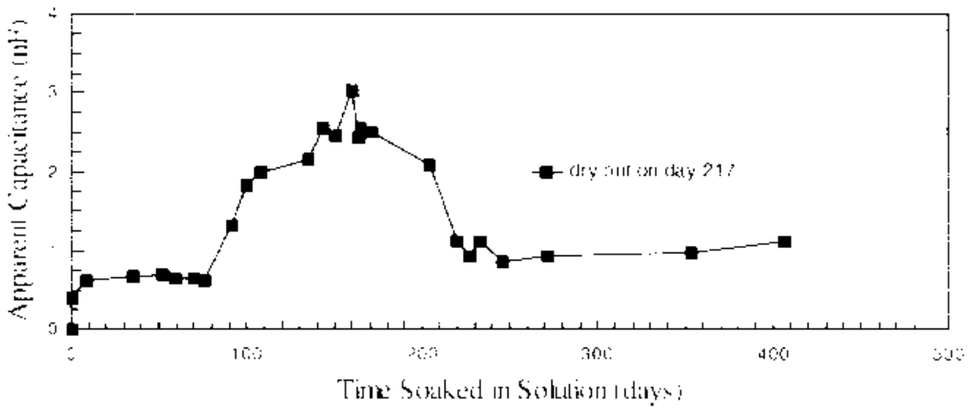

Figure 2-2 Apparent capacitance of site 1 on U. Michigan ribbon-cable probe No. 1 at 200 V/s for the 25 scan rate studies.

We do not have a satisfactory explanation for the increase in apparent capacitance between days 91 and 220. The inadvertent drying out of the electrode at day 217 presumably caused the decrease in C_{app}. However, there has been no increase in C_{app} similar to that observed at day 91 for the 189 days of soaking since the electrode was rehydrated at day 217. This result, and the abruptness of the increase observed at day 91, suggests that the increase in C_{app} is not due to an ongoing degradation process at the electrode site. A comparison of the voltammetric scans used in the calculation of C_{app} at 200 V/s for days 59, 160, and 354 is shown in Fig. 2-3. The 59 and 354 day scans are not significantly different with only a modest increase in current observed for the longer soaking time. This difference might be due to an increase in the surface area of Ir accessible to the electrolyte or the formation of iridium oxide due to prior electrochemical testing at expanded potential limits. In either case, some increase in C_{app} via either mechanism is anticipated and, overall, this site has exhibited a stable electrochemical response after more than one year of soaking in PBS.

For reference, the integrated ribbon cable probe used in the soak test is of the Schmidt-type with rectangular electrode sites nominally 13 μm x 38 μm. The Ir deposition was done with the non-self aligned process and some misalignment between the Ir and underlying bonding pad was noted by The University of Michigan group. One electrode from this batch, characterized by scanning electron microscopy at EIC, showed an ~0.5 μm misalignment. No unusual electrochemistry related to the misalignment was observed with this particular probe.

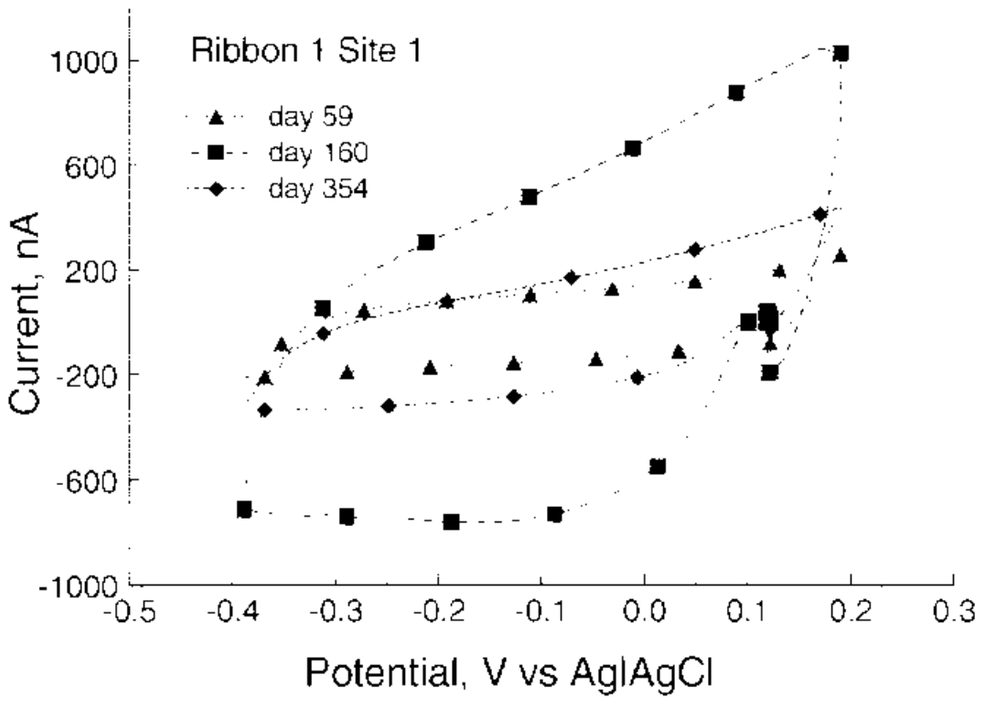

Figure 2-3 Voltammetric scans of site 1 on U. Michigan ribbon cable No. 1 after 59, 160, and 354 days of soaking.

3. IRIDIUM ACTIVATION STUDIES

3.1. Overview of Activation Studies

In neural prosthesis research, electrochemically formed iridium oxide films (AIROF) are widely accepted as a material for stimulation electrodes. A goal of this program is to develop a procedure to grow stable iridium oxide films that can be charged and discharged reversibly, *in vivo*, at current densities between 1 and 50 A/cm^2 of substrate geometric area. The charge requirement depends on the application and ranges from 200 μC/cm^2 to ~10 mC/cm^2.

Activated iridium oxide films have been studied extensively. Some suggestions have been put forward to explain the experimental observation of oxide accumulation, although the mechanism by which the AIROF grows and the details of the charge propagation mechanism are still unclear [1][2][3][4]. Nevertheless, it is known that thick anodic oxide films can be formed on the surface of an iridium electrode in an aqueous electrolyte by continuously cycling the electrode potential with a triangular or square waveform. The potential limits are between values slightly positive of

hydrogen evolution and just negative of the onset of oxygen evolution. It has been shown that AIROF formation is influenced by: the chemical composition of the electrolyte; the geometry and morphology of the iridium metal substrate; and, the duration and form of activation signal [5],[6]. The electrolyte composition influences the rate of formation as well as oxide morphology through the pH, the ionic strength, the conductivity and the structure of the double layer at the Ir/electrolyte interface [7].

During the potential or current controlled activation of Ir, a non-uniform current distribution occurs at the electrode. The current distribution is a function of the finite conductivity of the electrolyte, the electrode geometry, the porosity of the electrode material, and the details of the activation protocol (e.g. time, waveform, potential limits). These factors impact the rate of oxide formation, its morphology and the uniformity of the electrode coverage. Analytical solutions for the current distribution at electrodes with simple geometries are available but the description for the electrodes used in neural prostheses, at best, will be obtained numerically. Nevertheless, some prevailing trends for the current distribution can be qualitatively evaluated from existing solutions [8],[9]. Generally, current densities are lower at the less accessible part of the electrode. The current density distribution changes with time during the electrochemical transient for the charging process and after a certain time, the current density becomes uniform throughout the electrode [10]. The current density at the edge of an electrode may vary between infinity and zero depending on the angle between the insulator and conductor.

The effects of the non-uniform current distribution are seen experimentally during pulsed-potential activation of Ir. Thicker AIROF forms at the periphery of the electrode and may delaminate in a narrow band localized at the electrode edge (see Fig. 4-1). With continued activation, the region of delamination progresses from the periphery to the center of the electrode. More uniform AIROF can be obtained using pulsed activation waveforms with longer durations at each potential limit or with waveforms that switch more gradually between the limits. In the present quarter, the effects of pulse duration and the potential limits using square wave activation of Ir were evaluated.

3.2. Experimental Setup for Activation

The electrolytes used for activation and evaluation of AIROF were the following: phosphate-buffered saline (PBS), 0.08 M Na_2HPO_4 0.02 M NaH_2PO_4, and 0.12 M NaCl at pH 7.2; and 0.3 M Na_2HPO_4 at pH 9.1. The electrochemical cell was assembled in a 25 mL vial with a Kel-F cell top. The cell was equipped with a gas bubbler and a 0.05 cm diameter Pt wire counterelectrode. The Pt wire extended about 3 to 4 cm into the electrolyte to give an approximate area of 0.5 cm^2. A *Ag|AgCl(s)|Cl⁻ (3M KCl)* reference electrode (Microelectrodes Inc., No. MI-403), isolated from the main compartment by a salt bridge, was used for potential measurements. The potential of the reference electrode is 0.196 V vs. the normal hydrogen electrode (NHE) and -0.045 V vs. the saturated calomel electrode (SCE).

Two iridium electrodes were used for this portion of the activation study: a) an iridium disk (Bioanalytical Systems Inc) with nominal diameter of 127 μm and electrochemical surface area (ESA) of 1.4×10^{-4} cm^2, and b) an iridium disk fabricated at EIC by casting 1 mm diameter wire in Epon resin 828, (ESA, 7.89×10^{-3} cm^2). The electrochemical surface area of the electrodes was determined using multi-frequency cyclic voltammetric and chronoamperometric measurements of the diffusion controlled reduction of the ruthenium hexaammine ions [11]. Initially, between activation studies, the electrodes were polished mechanically to a mirror finish using 1 μm diamond paste. Subsequently, it was observed that this procedure caused a slight increase in ESA with each polishing, probably due to rounding at the edge of the Ir wire. Therefore, between each set of AIROF activation experiments, the electrodes were polished on a felt pad using no abrasive and only water as a lubricant. This procedure was effective in removing AIROF from the electrodes and produced Ir surfaces with similar voltammetric responses prior to each activation experiment.

The electrochemical instrumentation used was an Amel 551 potentiostat modulated by a PAR 175 Universal Programmer. For current measurements below the minimum sensitivity level of the Amel 551 potentiostat, a BAS Model PA 1 current amplifier was employed. Transients were recorded with a Bascom-Turner 5120 microprocessor controlled recorder and stored on floppy disks for analysis. The electrochemical cell was inside a Faraday cage during all the

electrochemical measurements. The cell was assembled and the solutions were deoxygenated with a flow of argon before any electrochemical measurements were made.

The oxide films were formed on the iridium electrodes by applying consecutive sets of 50 square wave potential pulses between fixed cathodic and anodic limits. After each set of 50 pulses, cyclic voltammograms were acquired at scan rates of 0.05 and 0.10 V/s between potential limits of -0.6 V and 0.8 V vs. Ag|AgCl. The anodic and cathodic charge storage capacities of the AIROF were determined by integrating the oxidation and reduction currents, respectively, during acquisition of the voltammograms. The unactivated Ir metal background was subtracted from the AIROF CV's before integration. Activation pulse widths from 0.5 s to 10 s were evaluated with various anodic and cathodic potential limits ranging between -0.35 to -0.8 V and 0.4 to 1.05 V, respectively. The potential waveform is shown schematically in Fig. 3-1. Figure 3-2 illustrates a typical CV response of iridium activated with a square-wave potential between limits of -0.60 V and +0.80 V with a pulse width of 10 s.

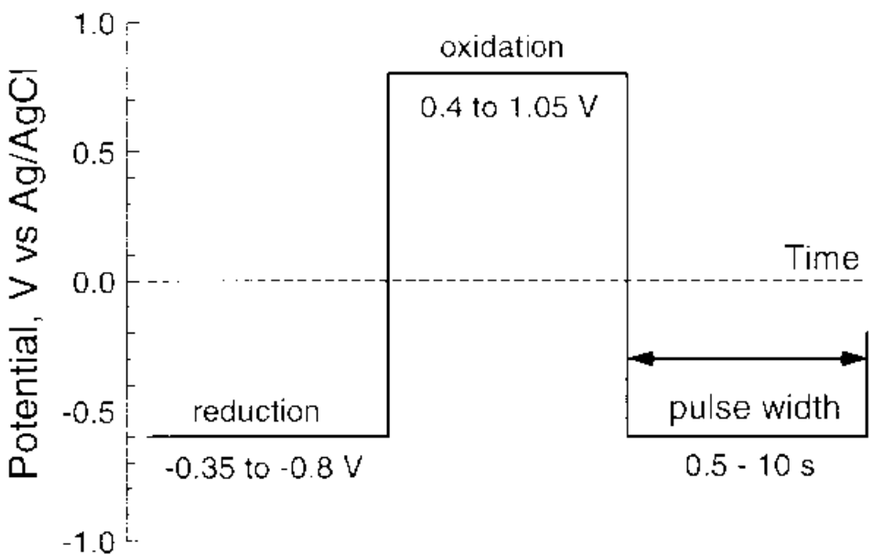

Figure 3-1 Potential waveform showing pulse width and potential limits used for activation of Ir. The waveform drawn is for limits of -0.6 V and 0.8 V vs. Ag|AgCl.

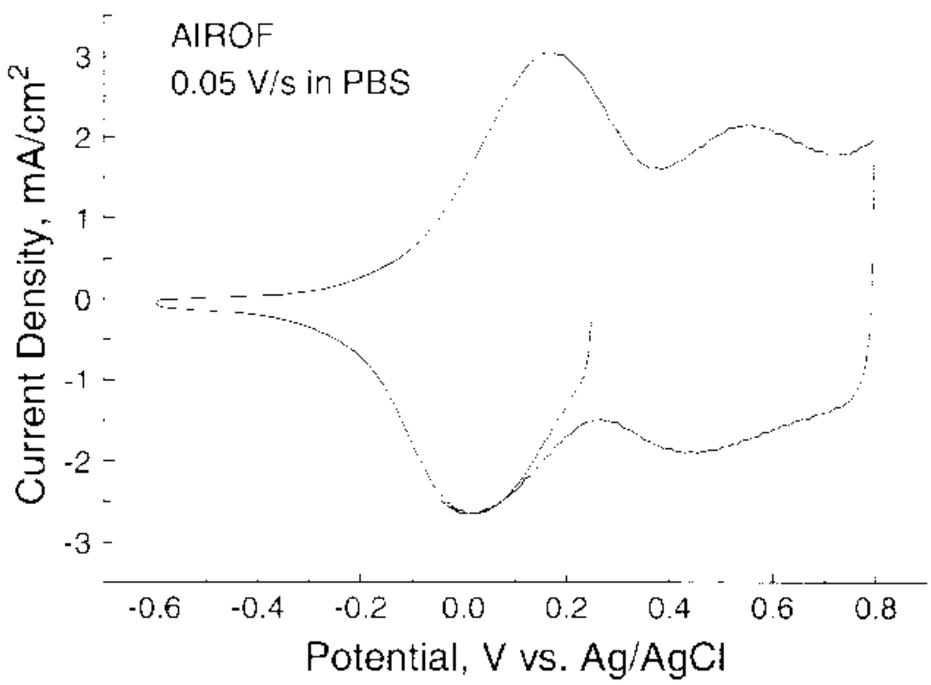

Figure 3-2 Cyclic voltammogram of a BAS Ir microelectrode at 0.05 V/sec in PBS. The electrode was activated in PBS for 1150 pulses between -0.6 V and 0.8 V at a pulse width of 10 s. The cathodic and anodic charge storage capacity are 43.9 and 43.6 mC/cm^2, respectively.

3.3. Effect of Pulse Width on Activation

Figure 3-3 illustrates the rate of Ir activation as a function of pulse number and pulse width for the BAS Ir electrode activated in 0.1M PBS. Data for pulse widths of 0.5, 2, 5, and 10 seconds are shown. As expected the longer pulse durations resulted in higher charge capacities. More importantly, for the longest pulses, the growth of oxide per cycle is constant at 0.036 mC/cm^2-pulse as shown by the least squares fit of cathodic charge storage capacity to activation pulse number in Fig. 3-4. A value of 0.218 mC/cm^2 was deduced by Woods [5] for the maximum CSC of AIROF produced in one activation cycle assuming 1 e$^-$ is involved in the AIROF reduction-oxidation process. The model proposed by Pickup and Birss is consistent with this value and sets a limit on the activation rate to a maximum of half a monolayer per cycle [4]. Since one monolayer is equivalent to ~0.54 mC/cm^2 of AIROF (for a 1 e$^-$ reaction), 15 activation pulses are required to convert one monolayer of the Ir metal substrate to AIROF with -0.6/0.8 V vs. Ag/AgCl pulses in PBS. In addition, a constant rate of oxide growth implies uniform AIROF

coverage. The departure from a constant rate of growth is more pronounced and occurs at lower charge storage capacities as the pulse duration decreases.

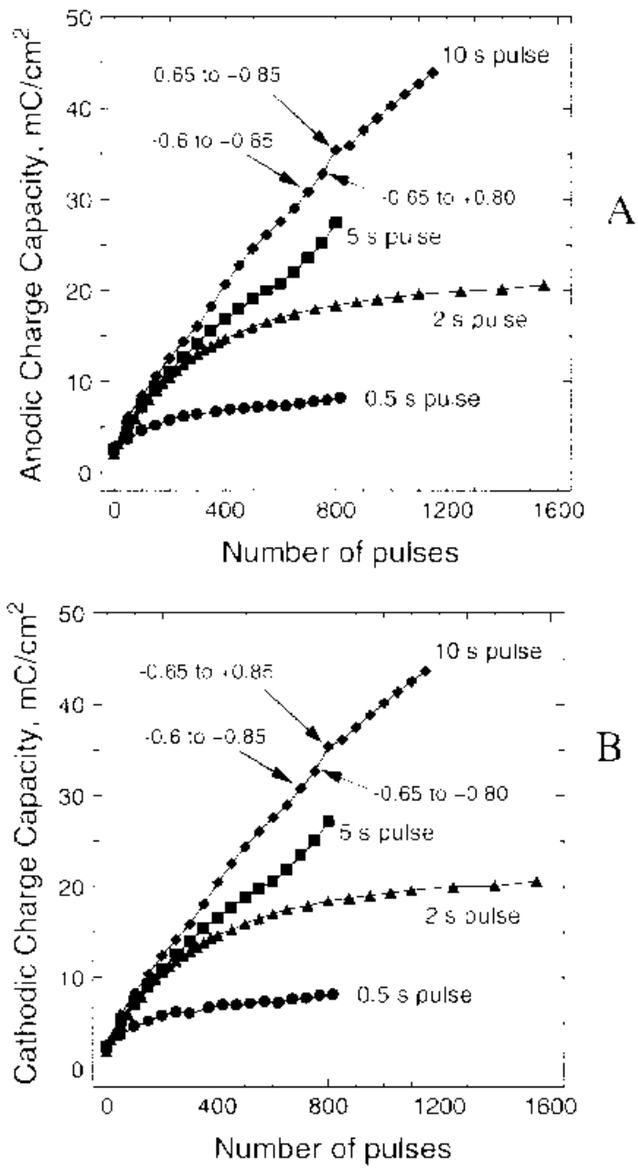

Figure 3-3 Anodic (A) and cathodic (B) charge capacities of AIROF activated at pulse widths of 0.5, 2, 5, and 10 s between limits of -0.6 and 0.8 V vs. Ag|AgCl. The arrows indicate points in the 10 s data for which subsequent activation limits were changed to those indicated.

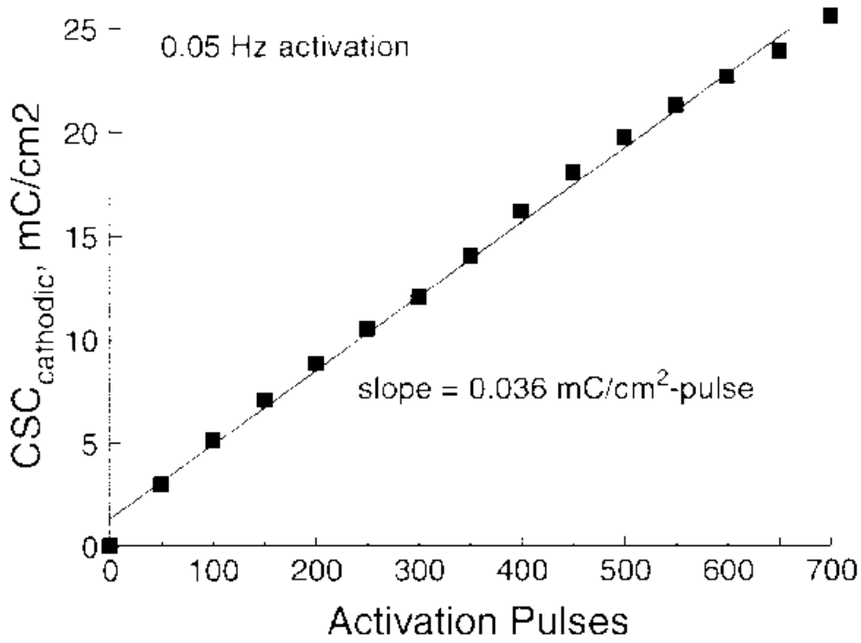

Figure 3-4 Cathodic CSC of AIROF activated at a pulse width of 10 s in PBS between limits of -0.6 V and 0.8 V vs. Ag|AgCl.

3.4. Influence of Activation Potential Limits On Charge Capacity

Because of the linearity in growth obtained with the 10 s pulse width and the presumed uniformity of the AIROF, this pulse width was chosen for subsequent studies on the effect of activation potential limits. The effect of the anodic potential limit, as it relates to charge capacity, was determined by applying consecutive sets of 50 potential pulses between a negative limit of -0.6 V and various positive potentials ranging from +0.40 V to +1.05 V vs. Ag|AgCl. After each set, cyclic voltammograms were acquired at scan rates 0.05 and 0.10 V/s using a potential window of -0.55 V to +0.75 V. Activation at each unique set of limits was carried out for 450 pulses. On completion of the activation, cyclic voltammograms were acquired at scan rates of 0.005, 0.05, 0.10 and 0.50 V/s. Figure 3-5 shows the cyclic voltammograms of AIROF activated between -0.6 V and selected anodic limits. The charge capacity after 450 pulses is shown in Fig. 3-6 as a function of the anodic limit. The capacity shows a steady increase up to a potential of 0.95V after which there is a marked decrease.

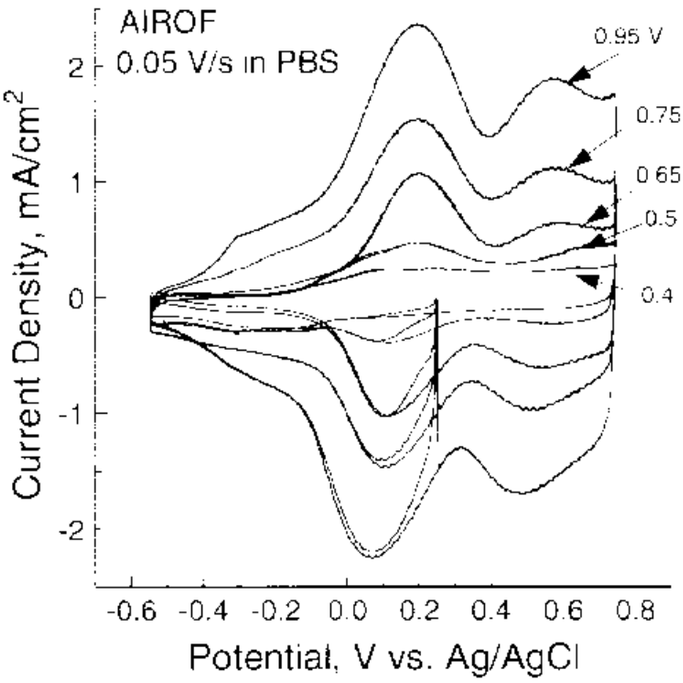

Figure 3-5 Cyclic voltammograms of AIROF activated for 450 pulses between -0.6 V and the anodic limits indicated. Voltammograms acquired at 0.05 V/s in PBS.

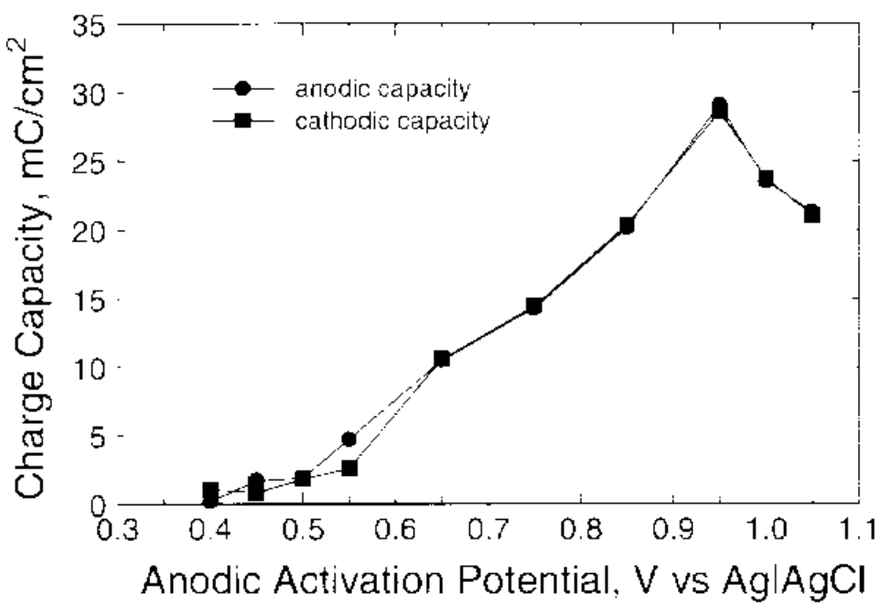

Figure 3-6 Charge capacity of AIROF as a function of anodic potential limit after activation for 450 pulses with a cathodic limit of -0.6 V. Charge capacities calculated from voltammograms acquired at 0.05 V/s between limits of -0.55 V and +0.75 V.

The affect of cathodic potential limit on AIROF activation was evaluated by holding the anodic potential at +0.80V while varying the cathodic potential between limits of -0.35 V and -0.80 V. Figure 3-7 shows the cyclic voltammetry for selected cathodic limits while Fig. 3.8 shows the charge capacity as a function of cathodic limit obtained from integration of the voltammograms. The charge capacity increases as the limit is made more negative until a value of -0.7 V is reached. At -0.75 V the capacity decreases. There is a further increase in capacity when the cathodic limit is pushed further negative to -0.80 V, but the CSC is still less than that obtained by activation at -0.7 V. A similar dip in the AIROF growth rate as a function of cathodic potential limit was observed previously by Pickup and Birss [12] who attribute the effect to a transition in local pH from acidic to alkaline as the cathodic limit is made more negative. Unusual oxidation peaks between 0.5-0.6 V are also apparent in the -0.8 V AIROF voltammogram. We suspect the oxidation peaks are related to reduction of dibasic sodium phosphate (NaH_2PO_4) which appears to have an onset at approximately -0.75 V vs. Ag|AgCl. We have observed reduction of NaH_2PO_4 on iridium, platinum and gold electrodes. This phenomenon is being investigated further

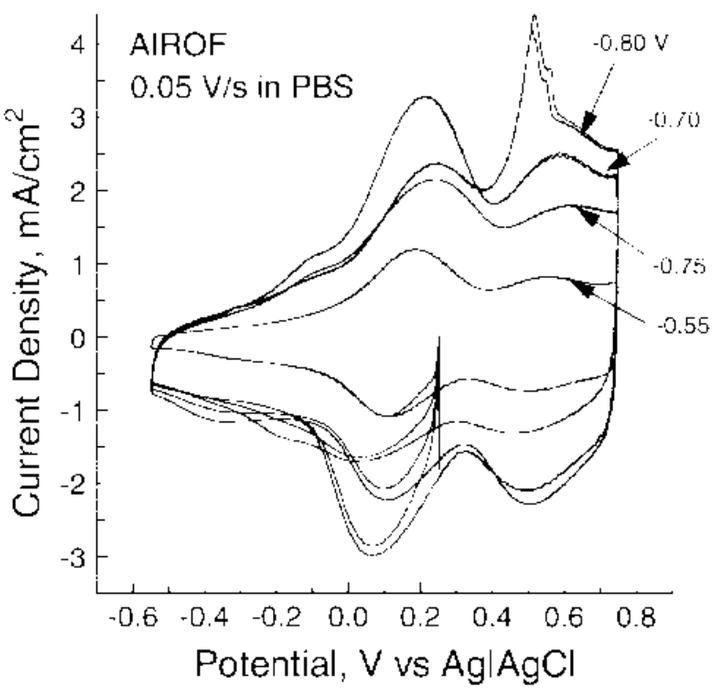

Figure 3.7 Cyclic voltammograms of AIROF activated for 450 pulses between 0.8 V and the cathodic limits indicated. Voltammograms acquired at 0.05 V/s in PBS.

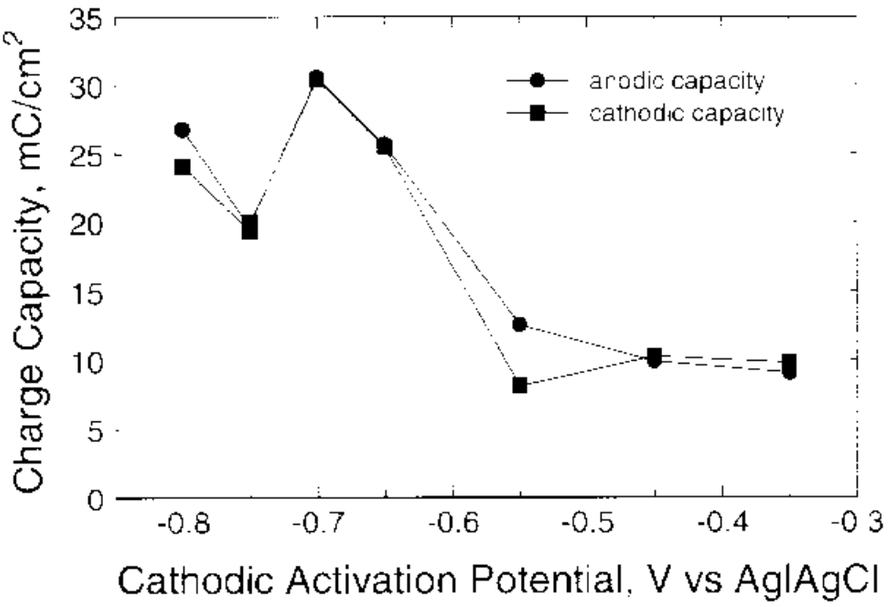

Figure 3-8 Charge capacity of AIROF as a function of cathodic potential limit after activation for 450 pulses with an anodic limit of 0.8 V. Charge capacities calculated from voltammograms acquired at 0.05 V/s between limits of 0.55 V and +0.75 V

3.5. AIROF Activation at Minimum and Maximum Growth Limits

From the previous data it is apparent that AIROF does not grow at anodic potential limits of 0.4 V or less when the cathodic limit is held at -0.6 V. Likewise, the oxide does not grow if the cathodic potential limit is -0.35 V (or more positive), when the anodic limit is held at 0.80 V. The maximum AIROF growth rate is expected for an anodic activation limit of 0.95V and a cathodic limit of -0.7 V.

In the following series of experiments, the combination of "minimum oxide growth" conditions, a potential window between -0.45 and +0.55V, is compared to our standard activation window (-0.60 to +0.80V), as well as the combination of "maximum oxide growth" conditions, a potential activation window between -0.70 and +0.95V. Additionally, windows slightly wider than the minimum and maximum conditions were tested. Again, activation was carried out by applying consecutive sets of 50 square-wave potential pulses with a pulse width of 10 s. After each set of 50 pulses, cyclic voltammograms were acquired at scan rates 0.05 and 0.10 V/s using a -0.55 V to +0.75 V potential window. Upon completion of 100, 450 and 1150 pulses, additional CVs were

taken at scan rates 0.005 and 0.50 V/s, and impedance spectroscopy was performed. Figure 3-9 shows the background corrected cyclic voltammograms after 1150 pulses for each of the four experiments discussed and for the standard conditions.

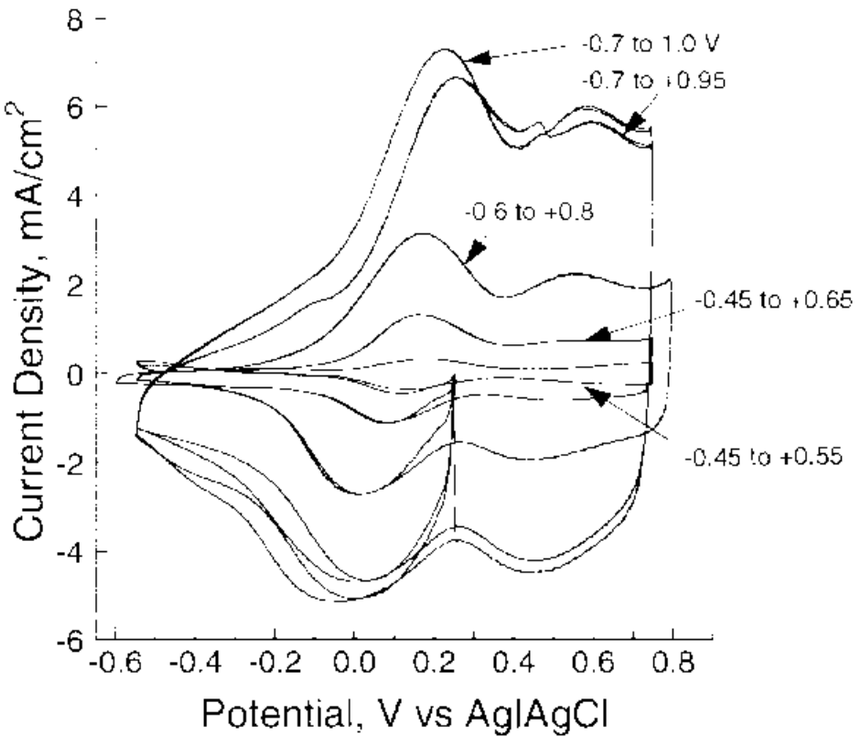

Figure 3-9 Cyclic voltammograms of AIROF activated with 1150, 10 s pulses between the potential limits indicated. The voltammograms were acquired in PBS at 0.05 V/s.

As shown in Figure 3-10, the data for cathodic charge capacity produced under "minimum" activation conditions show little increase with increasing pulse number, indicating no significant iridium oxide growth. Upon increasing the "minimum" activation window by 0.1 V at the anodic limit (-0.45 to 0.65 V), the data show a slight increase in capacity. The "maximum" activation window data show significantly more capacity, as well as a higher rate of oxide accumulation, than that shown by the standard activation window. The charge capacity of the AIROF activated with limits of -0.7/0.95 and -0.7/1.0 increased linearly over the first 450 pulses to a charge capacity of ~30 mC/cm^2. The activation rate in the linear region is 0.11 mC/cm^2 pulse, compared with 0.036 mC/cm^2 pulse observed for the -0.6/0.8 V limits. Increasing the "maximum" window

by 0.05V at the anodic limit did not produce AIROF with additional capacity. The anodic charge capacity mimics the behavior of the cathodic data and is not shown.

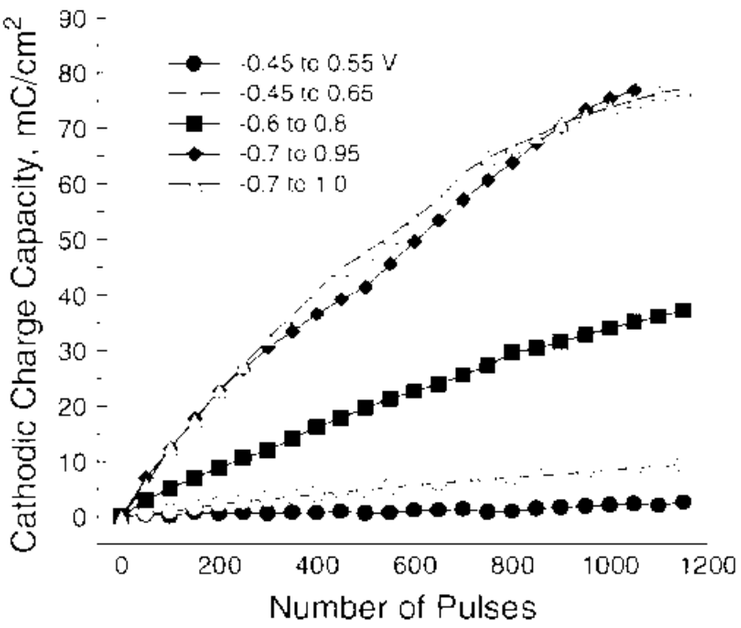

Figure 3-10 Cathodic charge capacity as a function of pulse number of AIROF activated by 10 s pulses at the potential limits indicated.

3.6. Influence Of Electrolyte on Ir Activation an AIROF Voltammetry

Previous work at EIC Laboratories showed that activation of Ir in 0.3 M Na_2HPO_4 (pH~9.1) produced AIROF capable of higher charge injection during biphasic stimulation pulses than AIROF activated in PBS (pH~7.2). This work was limited to an evaluation of a few activation protocols in each electrolyte and was not comprehensive enough to clearly identify one or the other electrolyte as being preferable. A comparison of activation rate in 0.3 M Na_2HPO_4 and PBS has been made using potential pulse activation between -0.6 V and 0.8 V in PBS and -0.7 V to 0.7 V in 0.3 M Na_2HPO_4 with pulse widths of 10 s. Figures 3-11 and 3-12 show the increase in anodic and cathodic charge capacity, respectively, over an 1150 pulse activation in each electrolyte.

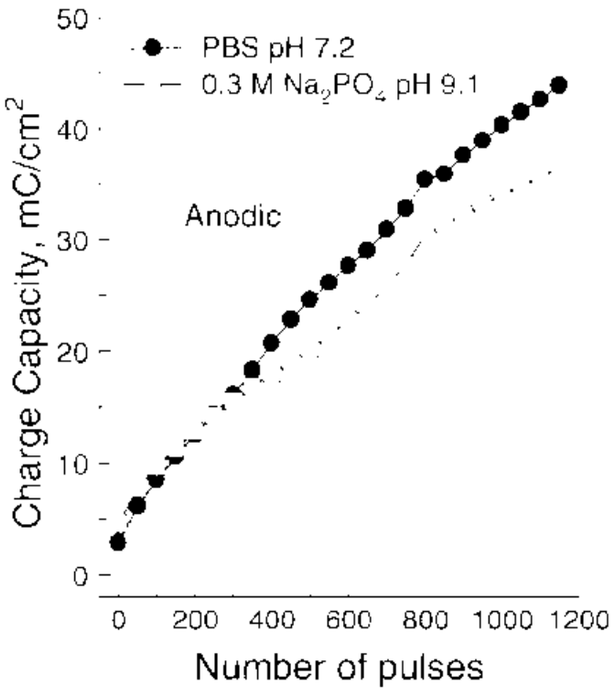

Figure 3-11 Comparison of the anodic charge capacity of AIROF activated in PBS and 0.3 M Na_2HPO_4.

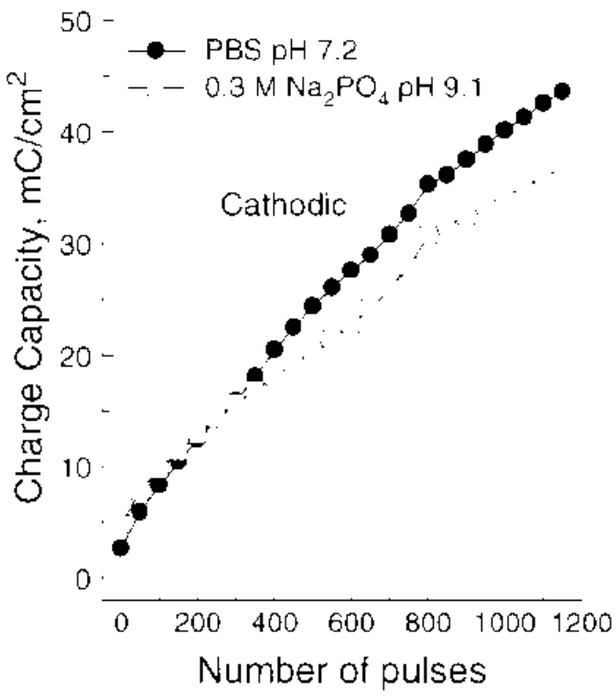

Figure 3-12 Comparison of the cathodic charge capacity of AIROF activated in PBS and 0.3 M Na_2HPO_4.

The rate of AIROF growth is comparable in PBS and 0.3 M Na_2HPO_4 after 250, 10 s pulses, corresponding to a charge capacity of ~16 mC/cm^2. With additional pulsing, the growth rate in PBS is marginally greater. Comparison of the cyclic voltammograms of the AIROF in each electrolyte, shown in Fig 3-13, reveals less separation of the primary reduction and oxidation waves of the Ir^{+3}/Ir^{+4} couple in PBS which is indicative of the higher buffering capacity of that electrolyte. The potential displacement is due to the difference in pH of the electrolytes.

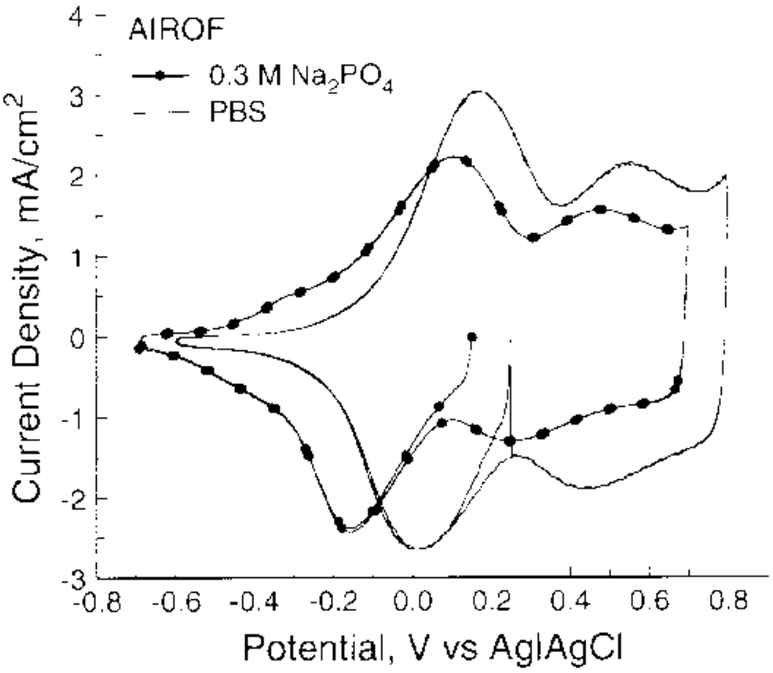

Figure 3-13 Comparison of cyclic voltammograms of AIROF activated for 1150, 10 s pulses in PBS and 0.3 M Na_2HPO_4.

The effect of buffer concentration on AIROF cyclic voltammetry is shown in Fig. 3-14. The NaCl concentration in each buffer was maintained at 7.36 g/l while the usual buffer concentration of 31.96 g/l $NaH_2PO_4.H_2O$ (monobasic sodium phosphate monohydrate) and 53.64 g/l $Na_2HPO_4.7H_2O$ (dibasic sodium phosphate heptahydrate) was incrementally decreased while keeping the ratio of monobasic to dibasic salt constant. Reducing the buffer concentration to 1/2 results in a very slight decrease in the peak current on the anodic waves and a more pronounced decrease in current and a potential shift of 50 mV in the negative direction on the primary reduction wave. As the buffer concentration is decreased further, the primary reduction wave is

reduced in magnitude and significantly broadened. The anodic waves at 0.2 V and 0.55 V (vs. SCE) are shifted slightly to more positive potentials with an ~20% reduction in the peak current. Similarly, the first reduction wave at 0.5 V is shifted slightly negative with a small decrease in peak current. Reducing the buffer concentration to 1/8 the initial value impacts the major Ir^{3+}/Ir^{4+} reduction wave quite significantly, while having only a minor effect on the other waves. In the absence of buffer, the familiar shape of the AIROF CV is completely lost and two widely spaced redox waves appear at -0.3 V and 0.5 V (vs. SCE). The charge available within the potential limits of the CV decreases with decreasing buffer concentration from 19 mC/cm^2 at full buffer to 12 mC/cm^2 with no buffer. Cycling the AIROF in nonbuffered electrolyte appears to have little permanent effect on the films as shown by the almost identical before and after CV's in fully buffered PBS. The comparison of the AIROF CV's in 0.3 M Na_2HPO_4 and PBS in Fig. 3-13 also shows a more pronounced shift in the potential of the primary reduction wave compared with the oxidation wave in the dibasic phosphate electrolyte relative to that observed in PBS.

Cyclic voltammetry of AIROF in a physiological electrolyte based on carbonate and phosphate buffers (137 mM NaCl, 29 mM $NaHCO_3$, 1.7 mM Na_2HPO_4, and 0.7 mM NaH_2PO_4 purged with a 5% CO_2/6% O_2/89% N_2 gas mixture to pH 7.41 is compared with that of PBS in Fig. 3-15. The CBS/PBS electrolyte has a buffer composition similar to that found in interstitial fluid. The response in the CBS/PBS appears intermediate between the 1/8 PBS and the no-buffer CV's shown in Fig. 3-14. There is a significant overvoltage for the primary Ir^{3+}/Ir^{4+} redox reaction with the maxima in the reduction and oxidation waves shifted to -0.15 V and 0.35 V (vs. SCE), respectively, compared with 0.0 V and 0.1 V (vs. SCE) for the same AIROF in PBS. There was a corresponding decline in charge capacity at 0.05 V/s from 18.9 mC/cm^2 in PBS to 11.2 mC/cm^2 in CBS/PBS.

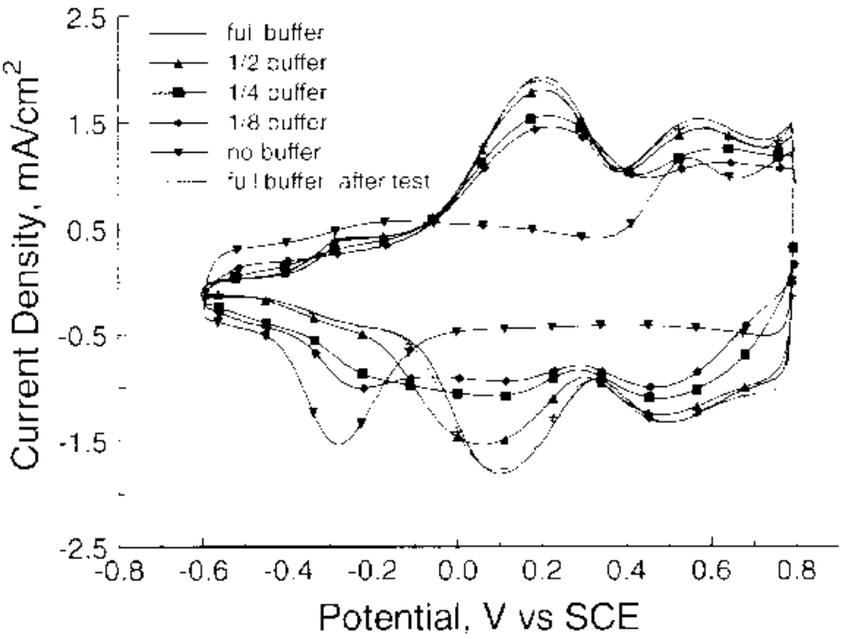

Figure 3-14 The effect of buffer concentration on the voltammetric response of AIROF in PBS at a scan rate of 0.05 V/s. The AIROF was activated by 0.5 s per phase potential pulsing in 0.3 M Na_2HPO_4 between limits of -0.8 V and 0.75 V vs. SCE prior to testing in PBS.

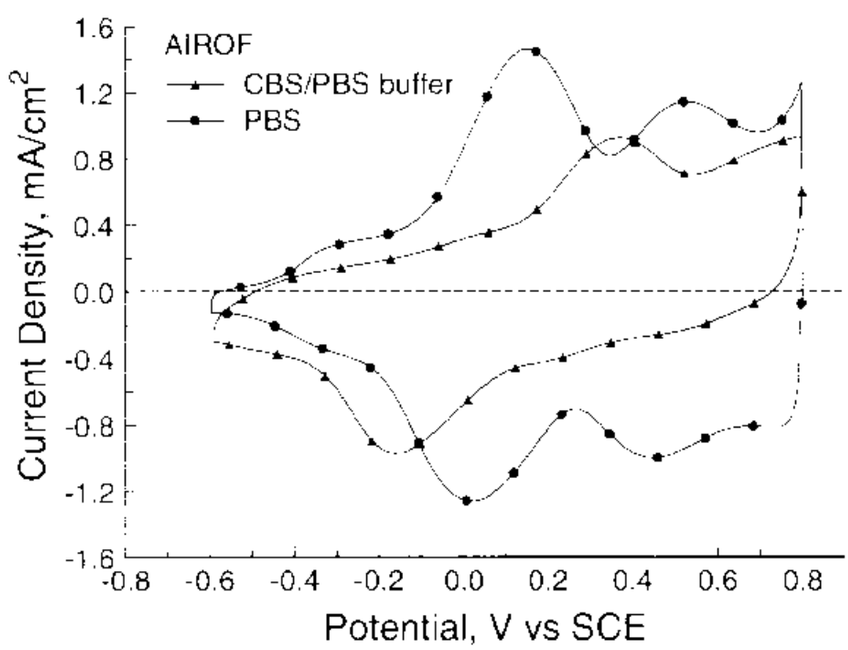

Figure 3-15 Comparison of AIROF cyclic voltammetry in physiological CBS/PBS and in PBS. Sweep rate 0.05 V/s.

3.7. Discussion of Activation Results

Studies of Ir activation indicate that oxide growth occurs at a rate that is always less than the oxidation of one monolayer of Ir metal and that cyclic oxidation and reduction is required to grow a film thicker than one monolayer. [12][13] With these constraints, potential pulsing will result in uniform oxide growth if the pulse width is sufficiently long that the oxidation and reduction currents have decayed to background levels before the next pulse is initiated. For the circular electrodes used in the present study, the oxide formation must follow the nonuniformity imposed by the primary current distribution. Therefore, oxide is formed at the exterior of the electrode and moves towards the center. If sufficient time at the potential limits is allowed, the oxide formation reactions reaches completion at the center and uniform activation is achieved. The completion of the reaction should coincide with a decay in the current to the background level which can be conveniently monitored with an oscilloscope.

The most favorable conditions for the efficient and uniform activation of iridium metal in 0.1M PBS are thus far: potential pulse with a 10 second half-wave duration between the potential limits -0.70 and +0.95 volts vs. the reference electrode. The data on Ir activation protocols presented for this quarter address activation rates and do not provide information about which protocols might produce AIROF with higher charge injection capacities. During the course of the activation study AC impedance data were collected for activation with different potential limits in PBS and for activation in 0.3 M NaH_2PO_4. The impedance data are being analyzed in an effort to quantify the transport properties of the AIROF as a basis for optimizing charge injection.

4. ELECTRODES WITH GRADED Ti-Ir INTERFACES

In the previous quarter we described work on thin-film, Ti-Ir electrodes deposited with discrete and compositionally graded interfaces. In QPR No. 8, the behavior of various Ti:Ir alloys, prepared by cosputtering, was evaluated by cyclic voltammetry during pulse activation and by scanning electron microscopy. Briefly, 100% Ir alloys activate to a cathodic charge storage capacity (CSC) of ~18 mC/cm^2 after 5,000 pulses as did the 79 % Ir alloy. For lower Ir concentrations, the CSC decreased, with only very slight activation apparent after 5,000 pulses in

the 35% Ir alloy and no activation in the 28% Ir alloy. Intermediate levels of activation were obtained with the 45% and 56% alloys. These data were used as a basis for designing TiIr films with graded interfaces.

4.1. Preparation of Compositionally Graded Ti-Ir Films

The Ti and Ir are deposited by DC sputtering using a multitarget apparatus that allows near-simultaneous sputtering from independently controllable sputtering guns. The apparatus was described in QPR No. 7. Alloy films are obtained by cosputtering from pure Ir and Ti targets. The composition of the films is controlled by adjusting the power to the sputtering guns and rotating the substrates under the targets at a sufficiently high rate that a homogeneous film is formed. Compositionally graded Ti-Ir interfaces are obtained by incrementing and decrementing the power to the individual sputter guns during deposition while maintaining a constant total sputtering current or power. Details of the deposition conditions are provided in QPR No. 8.

4.2. Activation of TiIr Alloys

Compositionally graded electrodes with an area of ~0.01-0.02 cm^2 were made by masking an approximately circular area of the sputtered films with epoxy. A quantitative measure of the area was then obtained using a digital camera with image analysis software. The electrodes were activated in 0.3 M Na_2HPO_4 (pH 9.1) or PBS (pH 7.2) using a potential pulse waveform with a 10 s dwell at each potential limit. In previous studies of the graded interface electrodes, an 0.5 s dwell had been used for activation. The short dwell time led to accelerated delamination of the AIROF at the edges of the electrode due to the nonuniform current distribution as shown in Fig. 4-1. A 10 s dwell was chosen to minimize nonuniform activation as described in Section 3.0. Cyclic voltammograms were taken periodically throughout the activation and the charge storage capacity calculated by integrating the cathodic or anodic current during an 0.05 V/s sweep between the activation potential limits.

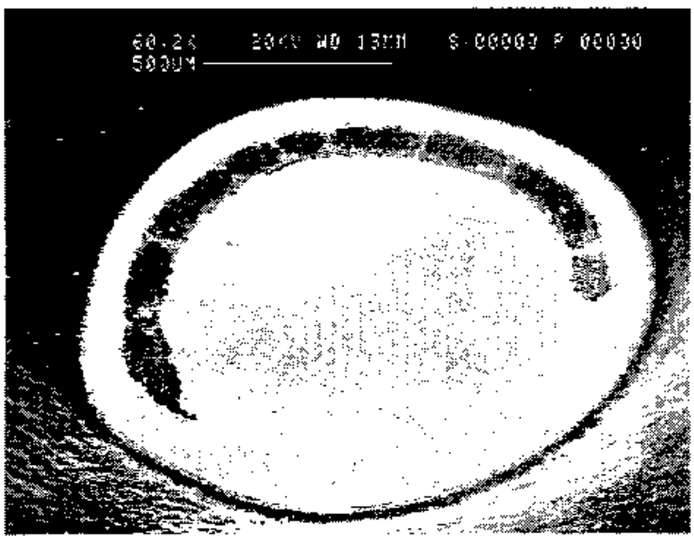

Figure 4-1. Typical delamination of AIROF around the perimeter of a 100% Ir, discrete-interface electrode, pulse activated in 0.3 M Na_2HPO_4 between limits of -0.755 V and 0.795 V vs. Ag/AgCl with an 0.5 s dwell at each limit.

4.3. Activation of Graded Interface Electrodes

The results of the activation study on graded interface electrodes are presented as composite figures that show the compositional profile of the electrode, periodic cyclic voltammograms, and the cathodic CSC as a function of pulse number. The results for a discrete interface electrode with a 50 nm thick film of 100% Ir on a 50 nm thick Ti adhesion layer activated in 0.3 M Na_2HPO_4 are shown in Fig. 4-2. The electrode activated to a CSC of 60 mC/cm^2 over 1600 pulses and then abruptly delaminated from the substrate. The delaminated AIROF had a dry thickness of 300 nm as measured by scanning electron microscopy (Fig 4-3), indicating at least a factor of 6 increase in film thickness as Ir is converted to AIROF. Some regions of the AIROF also showed a laminar growth morphology and blistering (Fig 4-4).

A similar result was obtained for a 70% Ir/30% Ti electrode with a discrete interface as shown in Fig. 4-5. After activation to 32 mC/cm^2 in 1,000 pulses, the AIROF delaminated. Initial scanning electron microscopy of the delaminated AIROF indicated a similar volume expansion in the 70% Ir alloy as the 100% Ir. A 60% Ir/40% Ti electrode with a discrete interface, however, did not delaminate after activation to 42 mC/cm^2 in 4,000 pulses (Fig. 4-6). At this point the activation was stopped. These electrodes are now being examined in more detail by scanning electron microscopy in an effort to identify the AIROF thickness and, for the 70% Ir electrode, determine whether delamination occurred at the Ti/TiIr alloy interface or within the activated film.

The results for two graded interface electrodes are shown in Figs. 4-7 and 4-8. The electrode shown in Fig 4-7 was compositionally graded over 70 nm and capped with 10 nm of pure Ir. The electrode activated to a maximum CSC of ~70 mC/cm² after 4000 activation pulses. A decline in CSC was observed with continued pulsing, decreasing to 50 mC/cm² at 10,000 pulses. There was no visible evidence of AIROF delamination although the decline in CSC indicates some loss of AIROF either through localized delamination or dissolution. An interesting feature of the activation behavior is the increase in CSC observed after the electrodes were allowed to rest quiescently in the electrolyte, typically overnight. The open circles in the CSC data in Fig. 4-7 show the CSC after the rest period. A difference in the CSC measured immediately after pulsing and after a period of quiescence becomes apparent after the CSC exceeds ~60 mC/cm² or is either not increasing or is slightly decreasing with pulsing. One exception was observed with the 70% Ir discrete interface electrode where a difference was observed at a CSC of 32 mC/cm² immediately before the AIROF delaminated. The electrode shown in Fig 4-8 was compositionally graded over 83 nm and capped with 20 nm of pure Ir. This electrode activated to a CSC of 80-90 mC/cm² after ~4,000 pulses and remained stable to 10,000 pulses at which point the activation was stopped.

5. FUTURE WORK

The evaluation of activation protocols will continue in the next quarter. Analysis of the impedance data acquired during the course of the activation study will be used to examine the affect of activation conditions on charge transport in an effort to establish protocols that optimize charge injection capacity. We anticipate investigating the affect of other activation parameters, such as charge storage capacity or thickness, on charge injection and utilization of AIROF. The evaluation of compositionally graded interfaces will continue with an evaluation of charge injection limits of electrodes activated using the optimum protocols established from the impedance study.

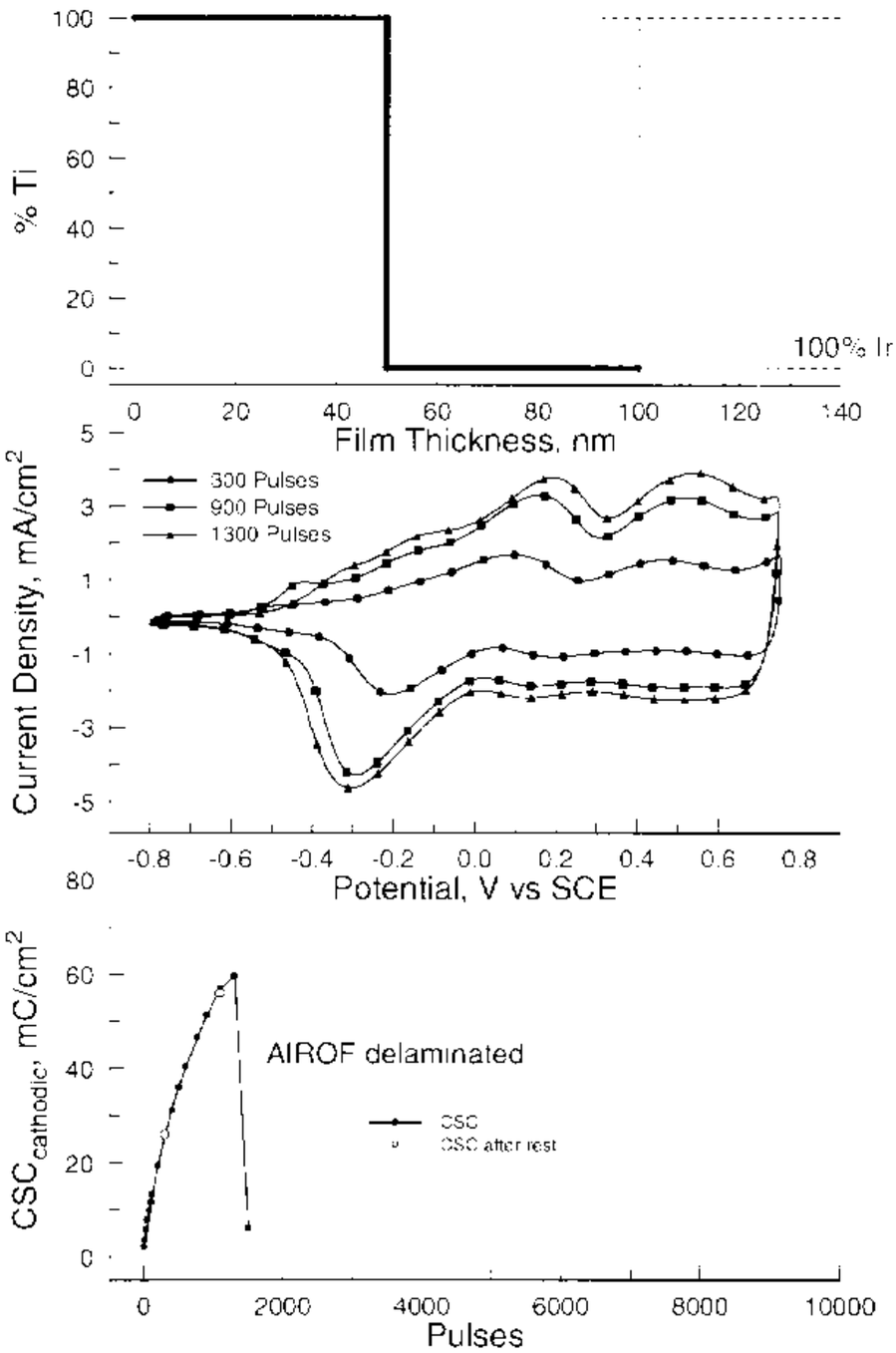

Figure 4-2. Results of the activation study of a 50 nm thick Ir electrode with a discrete interface. Activation was in 0.3 M Na_2HPO_4 between limits of -0.755 V and 0.795 V vs. Ag|AgCl with a 10 s dwell at each potential limit. SEM's of the failed electrode are shown in Figs 4-3 and 4-4.

Figure 4-3. Scanning electron micrograph of delaminated AIROF showing a 300 nm film thickness. The Ir film prior to activation was 50 nm thick.

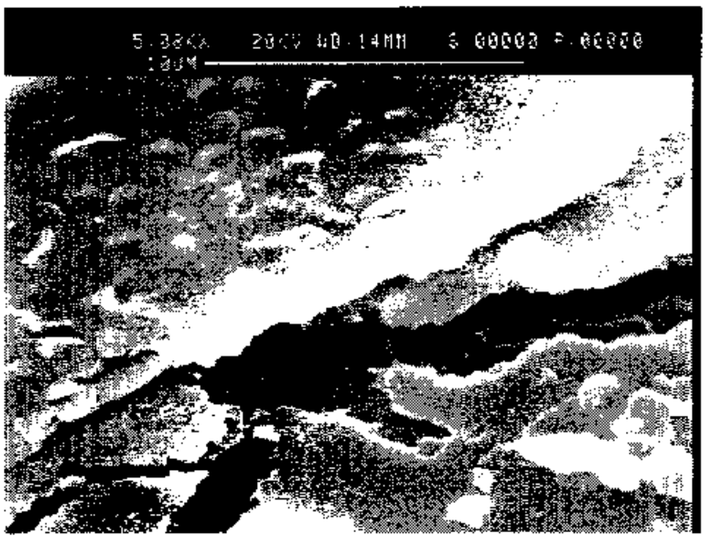

Figure 4-4. Scanning electron microscopy of AIROF delaminated from a Ti adhesion layer following 1600 activation pulses in 0.3 M Na_2HPO_4. The laminated structure of AIROF and blistering are apparent.

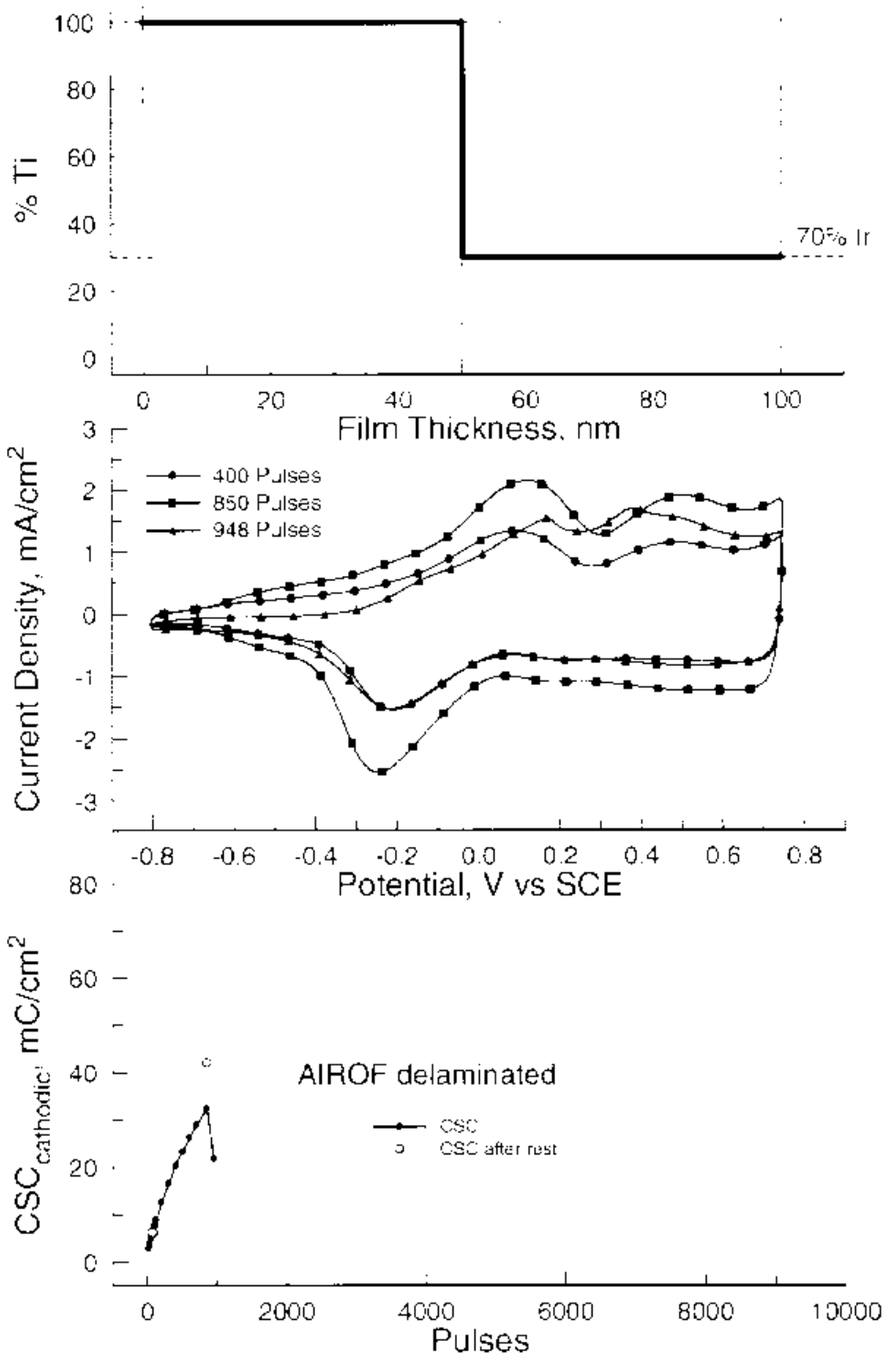

Figure 4-5. Results of the activation study of a 50 nm thick 70% Ir/30% Ti electrode with a discrete interface. Activation was in 0.3 M Na_2HPO_4 between limits of -0.755 V and 0.795 V vs. Ag|AgCl with a 10 s dwell at each potential limit.

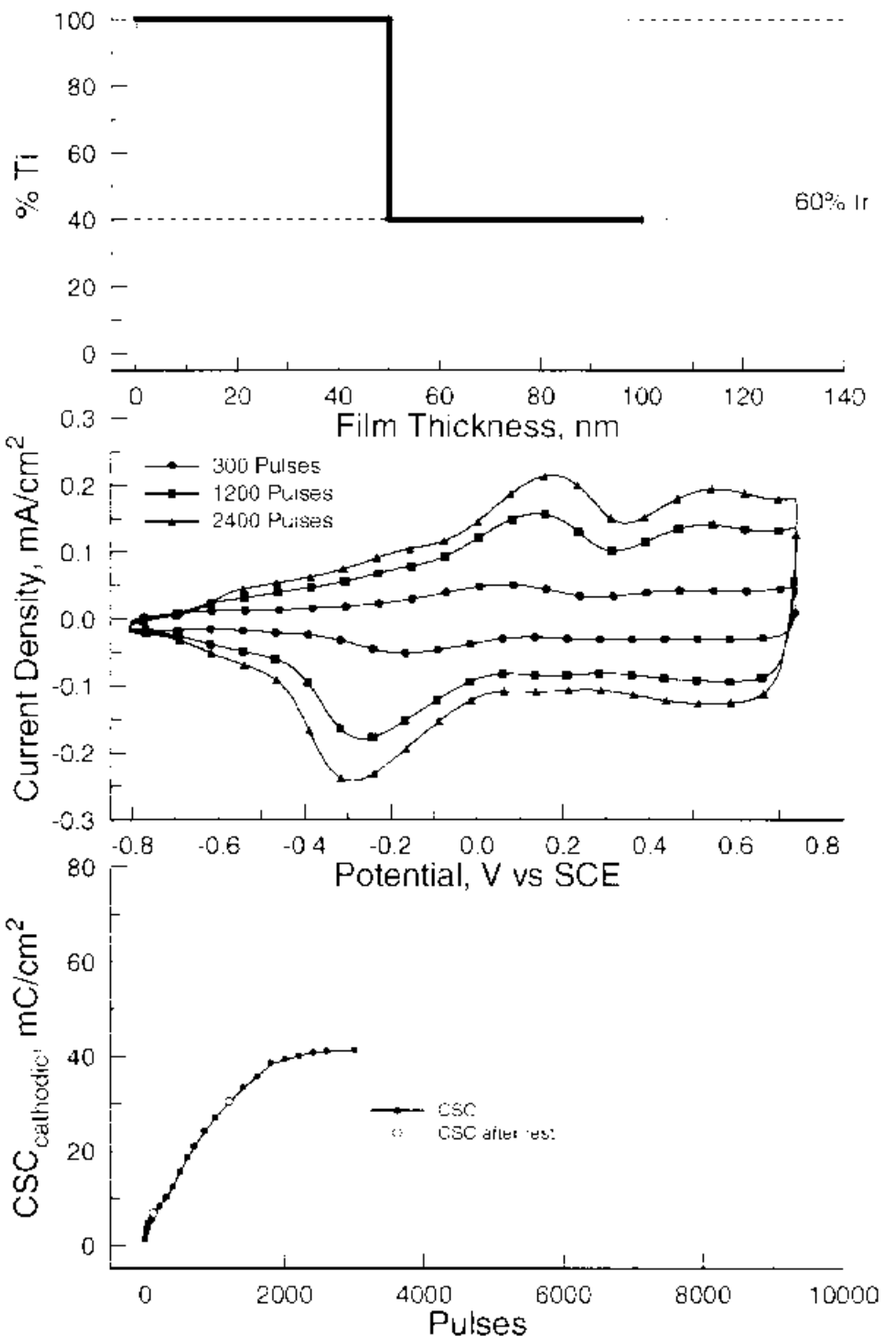

Figure 4-6. Results of the activation study of a 50 nm thick 60% Ir/40% Ti electrode with a discrete interface. Activation was in 0.3 M Na_2HPO_4 between limits of -0.755 V and 0.795 V vs. Ag/AgCl with a 10 s dwell at each potential limit.

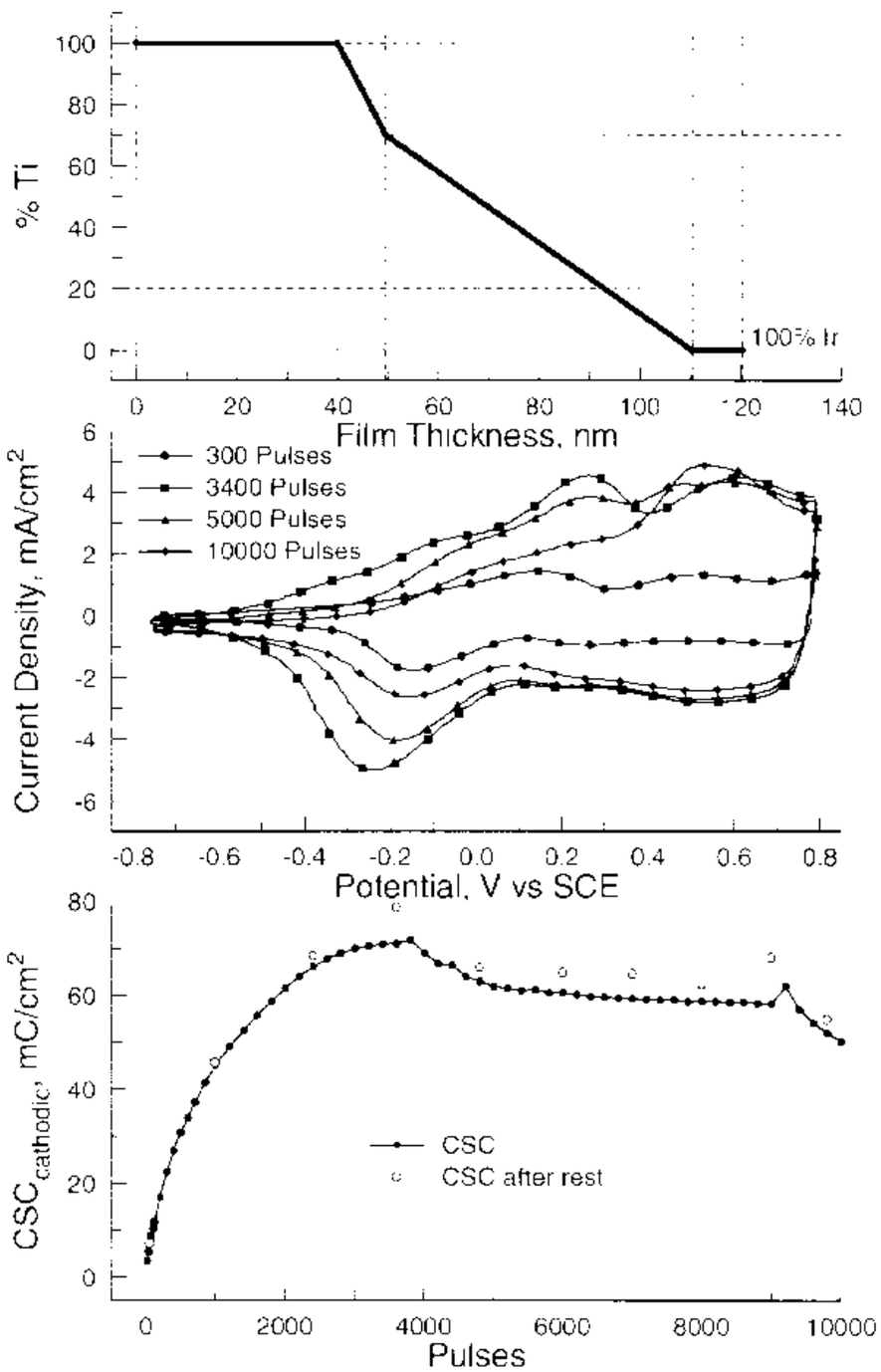

Figure 4-7. Results of the activation study of a graded interface electrode capped with 10 nm of Ir. Activation was in 0.3 M Na_2HPO_4 between limits of -0.755 V and 0.795 V vs. Ag/AgCl with a 10 s dwell at each potential limit

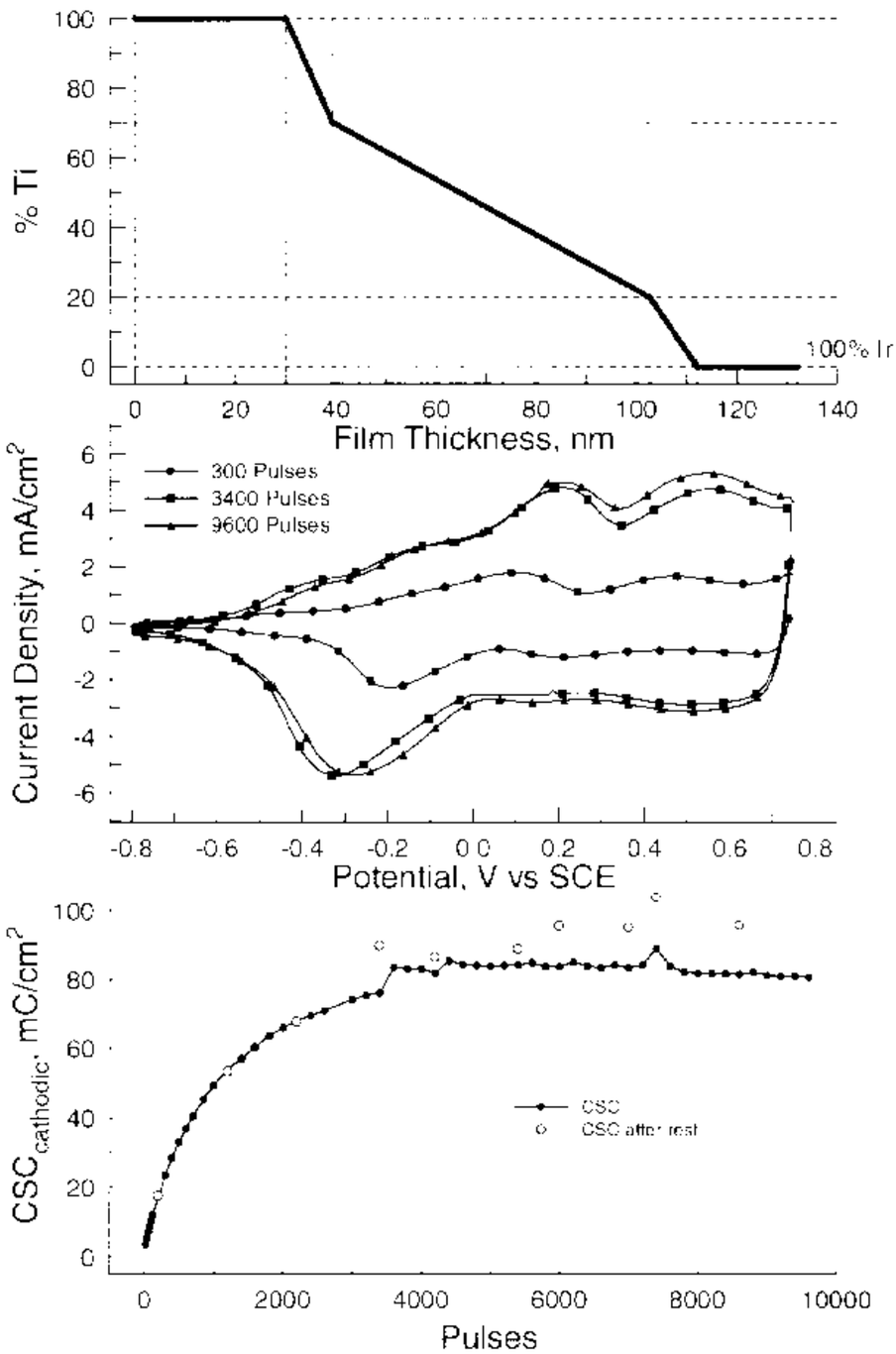

Figure 4-8 Results of the activation study of a graded interface electrode capped with 20 nm of Ir. Activation was in 0.3 M Na_2HPO_4 between limits of -0.755 V and 0.795 V vs. Ag|AgCl with a 10 s dwell at each potential limit.

6. REFERENCES

1. J. Mozota and B. E. Conway, "Modification of Apparent Electrocatalysis for Anodic Chlorine Evolution on Electrochemically Conditioned Oxide Films at Iridium Anodes," J. Electrochem. Soc., vol. 128, pp. 2143-2149, 1981.

2. L. D. Burke and R. A. Scannell, "An Investigation of Hydrous Oxide Growth on Iridium in Base," J. Electroanal. Chem., vol. 175, pp. 119-141, 1984.

3. D. N. Buckely and L. D. Burke, "The Oxygen Electrode Part 5. Enhancement of Charge Capacity if an Iridium Surface in the Anodic Region," J. Chem. Soc. Faraday Trans., vol. 71, pp. 1447-1459, 1975.

4. P. G. Pickup and V. I. Birss, "A Model for Anodic Hydrous Oxide Growth at Iridium," J. Electroanal. Chem., vol. 220, pp. 83-100, 1987.

5. R. Woods, "Hydrogen Adsorption on Platinum, Iridium and Rhodium Electrodes at Reduced Temperatures and the Determination of Real Surface Area," Electroanal. Chem. and Interfacial Electrochem.," vol. 49, pp. 217-226, 1974.

6. S. Gottesfeld and J. D. E. McIntyre, "Electrochromism in Anodic Iridium Oxide Films II. pH Effects on Corrosion Stability and the Mechanisms of Coloration and Bleaching," J. Electrochem. Soc., vol. 126, pp. 742-750, 1979

7. B. E. Conway, "Transition from 'Supercapacitor' to 'Battery' Behavior in Electrochemical Energy Storage," J. Electrochem. Soc., vol. 138, pp. 1539-1548, 1991.

8. M. F. Suesserman, F. A. Spelman, and J. T. Rubinstein, "*In Vitro* Measurement and Characterization of Current Density Profiles Produced by Nonrecessed, Simple Recessed, and Radially Varying Recessed Stimulating Electrodes," IEEE Tran. Biomed. Eng., vol. 38, pp. 401-408.

9. W. Tiedermann and J. Newman, "Double-Layer Capacity Determination of Porous Electrodes," J. Electrochem. Soc., vol. 122, pp. 70-78, 1975.

10. F. A. Posey and T. Morozumi, "Theory of Potentiostatic and Galvanostatic Charging of the Double Layer in Porous Electrodes," J. Electrochem. Soc., vol. 113, pp. 176-184, 1966.

11. U. M. Twardoch, "Integrity of Ultramicro-stimulation Electrodes Determined from Electrochemical Measurements," J. of Appl. Electrochem., vol. 24, pp. 835-857, 1994.

12. P. G. Pickup and V. I. Birss, "The Influence of the Aqueous Growth Medium on the Growth Rate, Composition, and Structure of Hydrous Iridium Oxide Films," J. Electrochem. Soc., vol. 135, pp. 126-133, 1988

13 J. Mozota and B. E. Conway, "Surface and Bulk Processes at Oxidized Iridium Electrodes - I. Monolayer Stage and Transition to Reversible Multilayer Oxide Film Behavior," Electrochimica Acta, vol. 28, pp. 1-8, 1983